Quantum defect theory for the orbital Feshbach resonance

Yanting Cheng,[1] Ren Zhang,[1,*] and Peng Zhang[2,3,4,†]

[1]*Institute for Advanced Study, Tsinghua University, Beijing 100084, China*

[2]*Department of Physics, Renmin University of China, Beijing 100872, China*

[3]*Beijing Computational Science Research Center, Beijing 100084, China*

[4]*Beijing Key Laboratory of Opto-electronic Functional Materials & Micro-nano Devices, Renmin University of China, Beijing 100872, China*

(Received 3 August 2016; published 23 January 2017)

In the ultracold gases of alkali-earth-metal-like atoms, a new type of Feshbach resonance, i.e., the orbital Feshbach resonance (OFR), has been proposed and experimentally observed in ultracold ^{173}Yb atoms [R. Zhang *et al.*, Phys. Rev. Lett. **115**, 135301 (2015)]. When the OFR of the ^{173}Yb atoms occurs, the energy gap between the open and closed channels is smaller by two orders of magnitude than the van der Waals energy. As a result, quantitative accurate results for the low-energy two-body problems can be obtained via multichannel quantum defect theory (MQDT), which is based on the exact solution of the Schrödinger equation with the van der Waals potential. In this paper we use MQDT to calculate the two-atom scattering length, effective range, and binding energy of two-body bound states for the systems with OFR. With these results we further study the clock-transition spectrum for the two-body bound states, which can be used to experimentally measure the binding energy. Our results are helpful for the quantitative theoretical and experimental research for the ultracold gases of alkali-earth-metal-like atoms with OFR.

DOI: 10.1103/PhysRevA.95.013624

I. INTRODUCTION

Feshbach resonance [1] is a powerful tool for the control of interaction between ultracold atoms [2]. In ultracold gases of alkali-metal atoms the magnetic Feshbach resonances are widely used for tuning of s-wave scattering lengths [2]. For the gases of ultracold alkali-earth-metal-like atoms, recently we found a new type of Feshbach resonance, i.e., the orbital Feshbach resonance (OFR) [3]. With the help of OFR, one can precisely control the s-wave scattering length between two fermionic alkali-earth-metal-like atoms in $^1S_0$ and $^3P_0$ electronic orbital states with different nuclear spin, by changing the magnetic field [3]. Orbital Feshbach resonance has been experimentally observed in the ultracold gases of ^{173}Yb atoms [4,5]. It is also shown that using the ultracold gases of alkali-earth-metal-like atoms with OFR, one can study several interesting problems, including the Kondo effect, the strong-interacting ultracold Fermi gases with narrow Feshbach resonance, and the Leggett mode [3,6–14].

When the OFR of ^{173}Yb atoms occurs, the energy gap between the open and the closed channel is about 10^5 Hz. It is, by two orders of magnitude, smaller than the characteristic energy of the interatom interaction (i.e., the van der Waals energy), which is of the order of 10^7 Hz [4,5,15,16]. As a result, a simple zero-range two-channel Huang-Yang pseudopotential can be used as an approximation for the interatom interaction [3,16]. In this model, the two-body interaction is described by two parameters, i.e., the scattering lengths $a_\pm$ for the two independent scattering channels $|\pm\rangle$, which will be defined below. It is estimated that for ^{173}Yb atoms the quantitative precision of the OFR point given by the two-channel Huang-Yang pseudopotential is about 80% [3,16].

To obtain more accurate results, one needs to take into account the effects from the finite-range van der Waals interaction potential. To this end, one can numerically solve the multichannel Schrödinger equation with a model interaction potential that behaves as a van der Waals potential in the long-range limit (e.g., the Lennard-Jones potential) [12]. Nevertheless, there is also an analytical approach for the multichannel low-energy two-body problem with a van der Waals potential, i.e., the multichannel quantum defect theory (MQDT) [17–20], which is based on the analytical solution of the single-channel Schrödinger equation with a van der Waals potential [21]. In ultracold atomic gas physics, this MQDT approach was originally developed for alkali-metal atoms. Previous research for these systems shows that when the interchannel energy gap is much smaller than the van der Waals energy, the result given by the MQDT is quantitatively very accurate [18,20]. Thus, this approach is also applicable for the ultracold alkali-earth-metal-like atoms with an OFR with small energy gaps between the open and the closed channels, e.g., the ultracold ^{173}Yb atoms.

In this paper, using the MQDT, we solve the low-energy two-body problems for alkali-earth-metal-like atoms with an OFR. We derive the analytical expressions of the two-atom scattering length and effective range [Eqs. (36) and (37)], as well as the algebraic equation satisfied by the binding energy of two-body bound state [Eq. (48)]. All the results are expressed in terms of the scattering length $a_\pm$ as well as the characteristic length β_6 of the van der Waals potential. Our results show that the OFR for ^{173}Yb atoms is a narrow resonance [7]. Using these results, we further investigate the clock-transition spectrum of these systems, which can be used for the experimental measurement of the binding energy. Our results are helpful for both theoretical and experimental study for ultracold alkali-earth-metal-like atoms with OFR.

The remainder of this paper is organized as follows. In Sec. II we show the MQDT approach for our system and calculate the two-atom s-wave scattering length and effective range. In Sec. III we calculate the binding energy and wave function of the two-atom bound state, as well as the clock-transition spectrum. A summary and discussion of our results

*rine.zhang@gmail.com

†pengzhang@ruc.edu.cn

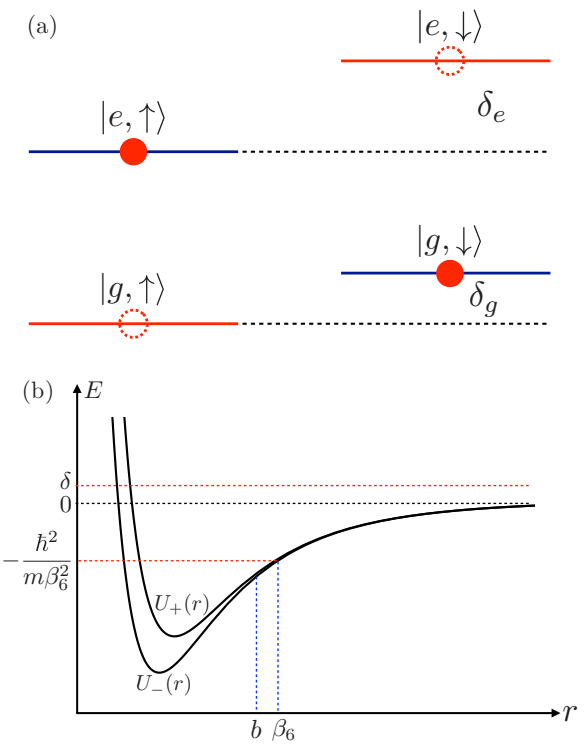

FIG. 1. (a) Energy-level diagram of a single atom. For the OFR, the open channel $|o\rangle$ is the two-body internal state with one atom in $|g,\downarrow\rangle$ and the other in $|e,\uparrow\rangle$ (the red closed circles), while the closed channel $|c\rangle$ is the state where one atom is in $|g,\uparrow\rangle$ and the other is in $|e,\downarrow\rangle$ (the red open dotted circles). Here $\delta_e = \mu_e(m_I' - m_I)B$ is the Zeeman energy difference between the single-atom states $|e,\downarrow\rangle$ and $|e,\uparrow\rangle$ and $\delta_g = \mu_g(m_I' - m_I)B$ is the one between states $|g,\downarrow\rangle$ and and $|g,\uparrow\rangle$. The Zeeman energy difference δ in Eq. (3) can be expressed as $\delta = \delta_e - \delta_g = (\delta\mu)B$, with $\delta\mu = (\mu_e - \mu_g)(m_I' - m_I)$. (b) Potential curves $U^{(\pm)}(r)$. In the region $r > b$, we have $U^{(+)}(r) \approx U^{(-)}(r) \approx -\hbar^2\beta_6^4/mr^6$. In our problem both the energy gap δ and the scattering energy ϵ are much smaller than $-\hbar^2/m\beta_6^2$.

are presented in Sec. IV. Details of our calculations are shown in the Appendixes.

II. SCATTERING LENGTH AND EFFECTIVE RANGE

We consider two fermionic alkali-earth-metal-like atoms in ${}^1S_0\,(g)$ and ${}^3P_0\,(e)$ electronic orbital states, with nuclear-spin magnetic quantum numbers m_I ($\uparrow$) and m_I' ($\downarrow$) (Fig. 1). The two-body internal state, with one atom in $|g,\downarrow\rangle$ and the other in $|e,\uparrow\rangle$, can be defined as

$$|o\rangle \equiv \frac{1}{\sqrt{2}}(|g\rangle^{(1)}|\downarrow\rangle^{(1)}|e\rangle^{(2)}|\uparrow\rangle^{(2)} - |e\rangle^{(1)}|\uparrow\rangle^{(1)}|g\rangle^{(2)}|\downarrow\rangle^{(2)}), \tag{1}$$

with $|e(g)\rangle^{(j)}$ $(j = 1,2)$ and $|\uparrow(\downarrow)\rangle^{(j)}$ $(j = 1,2)$ the electronic-orbital and nuclear-spin states of the jth atom, respectively. Similarly, we also define the state with one atom in $|g,\uparrow\rangle$ and the other in $|e,\downarrow\rangle$ as

$$|c\rangle \equiv \frac{1}{\sqrt{2}}(|g\rangle^{(1)}|\uparrow\rangle^{(1)}|e\rangle^{(2)}|\downarrow\rangle^{(2)} - |e\rangle^{(1)}|\downarrow\rangle^{(1)}|g\rangle^{(2)}|\uparrow\rangle^{(2)}). \tag{2}$$

The Hamiltonian for the two-atom relative motion is given by

$$\hat{H} = -\frac{\hbar^2}{m}\nabla_{\mathbf{r}}^2 + \delta|c\rangle\langle c| + U(r), \tag{3}$$

where m is the single-atom mass, $\mathbf{r}$ is the relative position of these two atoms, and

$$\delta = (\delta\mu)B$$

is the Zeeman energy difference between states $|c\rangle$ and $|o\rangle$, with $\delta\mu$ and B the magnetic moment difference of these two states and the magnetic field, respectively. Here $\delta\mu$ can be expressed as

$$\delta\mu = (\mu_e - \mu_g)(m_I' - m_I),$$

where $\mu_{e(g)}$ is the magnetic moment for the electronic orbital state $|e\rangle$ ($|g\rangle$). Without loss of generality, here we assume that $\delta\mu > 0$. In Eq. (3) $U(r)$ is the interatom interaction potential. It is diagonal in the bases

$$|\pm\rangle = \frac{1}{\sqrt{2}}(|c\rangle \mp |o\rangle) \tag{4}$$

and can be expressed as

$$U(r) = U^{(+)}(r)|+\rangle\langle+| + U^{(-)}(r)|-\rangle\langle-|, \tag{5}$$

where $U^{(\pm)}(r)$ is the potential curve with respect to state $|\pm\rangle$ [Fig. 1(b)]. When the two atoms are far away enough from each other, $U^{(\pm)}(r)$ can be approximated as the same van der Waals potential, i.e., we have

$$U^{(+)}(r > b) \approx U^{(-)}(r > b) \approx -\frac{\hbar^2\beta_6^4}{mr^6}. \tag{6}$$

Here β_6 is the characteristic length of the van der Waals potential and the range b satisfies the condition

$$b < \beta_6. \tag{7}$$

In this paper we focus on the systems where the energy gap δ between the states $|c\rangle$ and $|o\rangle$ is much smaller than the van der Waals energy $\hbar^2/m\beta_6^2$. As shown below, our finial result is independent of the exact value of b.

We consider the s-wave scattering of two atoms incident from channel $|o\rangle$, with relative momentum $\hbar k$. Here we assume that the scattering energy

$$\epsilon = \frac{\hbar^2k^2}{m} \tag{8}$$

is smaller than the interchannel energy gap δ. As a result, in the scattering process the channel $|o\rangle$ is open, while the channel $|c\rangle$ is closed.

The s-wave scattering length and effective range are determined by the two-atom scattering wave function $|\psi_{\epsilon,\delta}(r)\rangle$, which satisfies the Schrödinger equation

$$\hat{H}|\psi_{\epsilon,\delta}(r)\rangle = E|\psi_{\epsilon,\delta}(r)\rangle \tag{9}$$

with the boundary conditions

$$\lim_{r\to 0}[r|\psi_{\epsilon,\delta}(r)\rangle] = 0 \tag{10}$$

and

$$\lim_{r\to\infty}\langle c|\psi_{\epsilon,\delta}(r)\rangle = 0. \tag{11}$$

We point out that if we solve Eq. (9) only with the the boundary condition (10), we can get *two* linearly independent special solutions. The solution of Eq. (9) and conditions (10) and (11), i.e., the scattering wave function $|\psi_{\epsilon,\delta}(r)\rangle$, can be expressed as the superposition of these two special solutions. Following the idea of MQDT, below we will first derive the two special solutions of Eq. (9) and the condition (10) for the simple case with $\delta = 0$ and then derive the two special solutions of (9) and (10) for nonzero δ. Finally, we will construct the scattering wave function $|\psi_{\epsilon,\delta}(r)\rangle$ with these special solutions and the condition (11). With this wave function we can derive the s-wave scattering phase shift, scattering length, and effective range.

A. Special solutions of Eqs. (9) and (10) for $\delta = 0$

When $\delta = 0$, the Hamiltonian $\hat{H}$ given by Eq. (3) is diagonal in the bases $\{|+\rangle,|-\rangle\}$. Therefore, in this case we can choose the two special solutions of Eq. (9) and (10) as

$$|\psi^{(+)}_{\epsilon,\delta=0}(r)\rangle = \frac{\phi^{(+)}_\epsilon(r)}{r}|+\rangle, \tag{12}$$

$$|\psi^{(-)}_{\epsilon,\delta=0}(r)\rangle = \frac{\phi^{(-)}_\epsilon(r)}{r}|-\rangle. \tag{13}$$

Substituting Eqs. (12) and (13) into Eq. (9), we obtain two equations for the components $\phi^{(\pm)}_\epsilon(r)$:

$$-\frac{\hbar^2}{m}\frac{d^2}{dr^2}\phi^{(\pm)}_\epsilon(r) + U^{(\pm)}(r)\phi^{(\pm)}_\epsilon(r) = \epsilon\phi^{(\pm)}_\epsilon(r). \tag{14}$$

Furthermore, using the expression (6) of the potential $U^{(\pm)}(r)$ in the region $r > b$, in this region we can reduce these two equations to

$$-\frac{d^2}{dr^2}\phi^{(\pm)}_\epsilon(r) - \frac{\beta_6^4}{r^6}\phi^{(\pm)}_\epsilon(r) = \frac{m\epsilon}{\hbar^2}\phi^{(\pm)}_\epsilon(r). \tag{15}$$

Thus, when $r > b$ the components $\phi^{(\pm)}_\epsilon(r)$ can be expressed as the superpositions of two special solutions $f^0_\epsilon(r)$ and $g^0_\epsilon(r)$ of Eq. (15), which were analytically derived by Gao in Ref. [21]. These two solutions have energy-independent normalization in the limit $r \to 0$, as described in Eqs. (17) and (18) of Ref. [21] and illustrated in Fig. 2.

According to the above discussion, we can choose $\phi^{(\pm)}_\epsilon(r)$ to satisfy

$$\phi^{(\pm)}_\epsilon(r) = f^0_\epsilon(r) - K^0_\pm g^0_\epsilon(r) \quad \text{for } r > b. \tag{16}$$

The properties of the parameters $K^0_\pm$ can be investigated with the following two facts. First, in the region with $r \lesssim \beta_6$ the interaction potentials $U^{(\pm)}(r)$ are potential wells with the depth being on the order of the van der Waals energy $\hbar^2/m\beta_6^2$ or even larger. Thus, for our case with $\epsilon \ll \hbar^2/m\beta_6^2$ the behaviors of $\phi^{(\pm)}_\epsilon(r \lesssim \beta_6)$ are almost independent of ϵ. Explicitly, for $r \lesssim \beta_6$ the functions $\phi^{(\pm)}_\epsilon(r)$ can be formally expressed as $\phi^{(\pm)}_\epsilon(r) = F^{(\pm)}(\epsilon)R^{(\pm)}(r)$, whereas the functions $F^{(\pm)}(\epsilon)$ are independent of r and $G^{(\pm)}(r)$ are independent of ϵ. Second, the expressions of $f^0_\epsilon(r)$ and $g^0_\epsilon(r)$ [21] show that these two functions are also almost ϵ independent when $r \lesssim \beta_6$ for $\epsilon \ll \hbar^2/m\beta_6^2$, as illustrated in Fig. 2. Applying these two facts and Eq. (16) in the region $b < r \lesssim \beta_6$, we can obtain the conclusion that $F^{(\pm)}(\epsilon) = 1$ and the parameters $K_\pm$ are also almost independent of ϵ. That is one of the basic ideas of quantum defect theory [17,22,23].

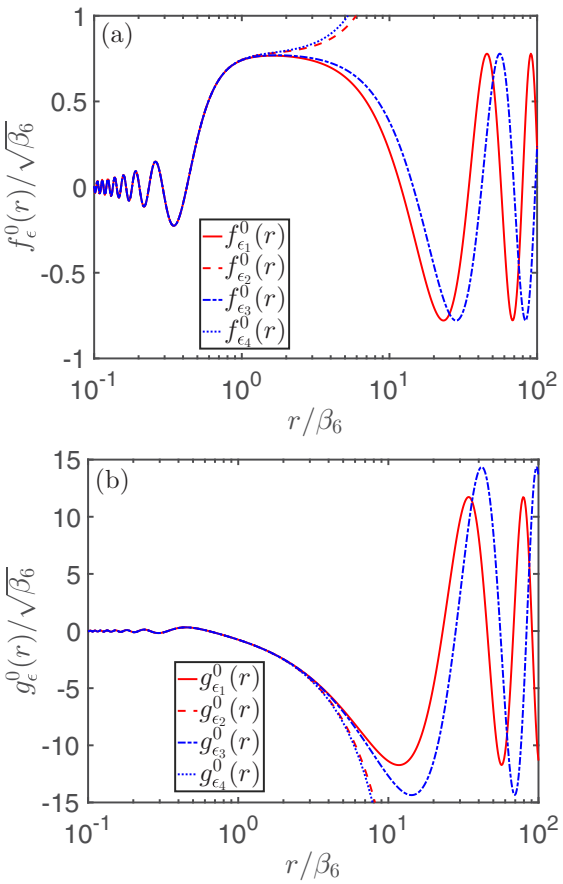

FIG. 2. Special solutions (a) $f^0_\epsilon(r)$ and (b) $g^0_\epsilon(r)$ of Eq. (15), derived by Gao in Ref. [21]. Notice that in Ref. [21] the equation is solved for both positive and negative values of ϵ. Here we show the results for the cases with ϵ taking the values $\epsilon_1 \equiv 0.019\hbar^2/m\beta_6^2$, $\epsilon_2 \equiv -0.019\hbar^2/m\beta_6^2$, $\epsilon_3 \equiv 0.013\hbar^2/m\beta_6^2$, and $\epsilon_4 \equiv -0.026\hbar^2/m\beta_6^2$. When $|\epsilon|$ is much smaller than $\hbar^2/m\beta_6^2$, in the region $r \lesssim \beta_6$ both $f^0_\epsilon(r)$ and $g^0_\epsilon(r)$ are almost independent of the values of ϵ.

For $\epsilon > 0$, in the limit $r \to \infty$ the functions $f^0_\epsilon(r)$ and $g^0_\epsilon(r)$ satisfy [21]

$$\lim_{r\to\infty} f^0_\epsilon(r) = \sqrt{\frac{2}{\pi k}}[Z_{ff}(\epsilon)\sin(kr) - Z_{fg}(\epsilon)\cos(kr)], \tag{17}$$

$$\lim_{r\to\infty} g^0_\epsilon(r) = \sqrt{\frac{2}{\pi k}}[Z_{gf}(\epsilon)\sin(kr) - Z_{gg}(\epsilon)\cos(kr)] \tag{18}$$

and the functions $Z_{ij}(\epsilon)$ $(i,j = f,g)$ are given in Ref. [21]. Substituting Eqs. (17) and (18) into Eq. (16) and using the expressions of $Z_{ij}(\epsilon)$, one can obtain

$$\lim_{r\to\infty} \phi^{(\pm)}_{\epsilon=0}(r) \propto \left[r - \frac{(2\pi)(K^0_\pm - 1)}{\Gamma(1/4)^2 K^0_\pm}\beta_6\right]. \tag{19}$$

That result was derived by Gao as Eq. (9) of Ref. [17]. On the other hand, since in our case with $\delta = 0$ the states $|+\rangle$

and $|-\rangle$ are two independent scattering channels, we also have $\lim_{r\to\infty}\phi^{(\pm)}_{\epsilon=0}(r)\propto(r-a_s^{(\pm)})$, where $a_s^{(\pm)}$ is the s-wave scattering length for each channel. Thus, Eq. (19) implies the relation between parameter $K^0_\pm$ and the scattering length $a_s^{(\pm)}$ [17]:

$$K^0_\pm=\frac{2\pi\beta_6}{2\pi\beta_6-a_s^{(\pm)}\Gamma(1/4)^2}. \tag{20}$$

B. Special solutions of Eqs. (9) and (10) for $\delta\neq 0$

Now we consider the special solutions of Eq. (9) and condition (10) for the case with $\delta\neq 0$. As mentioned above, in this section we ignore the boundary condition (11). When $\delta\neq 0$, it is convenient to expand $|\psi_{\epsilon,\delta}(r)\rangle$ in the bases $\{|c\rangle,|o\rangle\}$. Since the potential $U^{(\pm)}(r)$ satisfies the condition (6), for $r>b$ the interaction U is independent of the internal state of these two atoms and thus the channels $|c\rangle$ and $|o\rangle$ are decoupled and Eq. (9) can be simplified as

$$\left[-\frac{d^2}{dr^2}-\frac{\beta_6^4}{r^6}\right][r\langle o|\psi_{\epsilon,\delta}(r)\rangle]=\epsilon[r\langle o|\psi_{\epsilon,\delta}(r)\rangle], \tag{21}$$

$$\left[-\frac{d^2}{dr^2}-\frac{\beta_6^4}{r^6}\right][r\langle c|\psi_{\epsilon,\delta}(r)\rangle]=(\epsilon-\delta)[r\langle c|\psi_{\epsilon,\delta}(r)\rangle]. \tag{22}$$

Therefore, similar as in Sec. II A, for $r>b$ the component $r\langle o|\psi_{\epsilon,\delta}(r)\rangle$ can be expressed as the superpositions of functions $f^0_\epsilon(r)$ and $g^0_\epsilon(r)$, and $r\langle c|\psi_{\epsilon,\delta}(r)\rangle$ can be expressed as the superpositions of $f^0_{\epsilon-\delta}(r)$ and $g^0_{\epsilon-\delta}(r)$. Thus, we can choose the two special solutions of $|\psi^{(\alpha,\beta)}_{\epsilon,\delta}(r)\rangle$ of Eq. (9) to satisfy

$$\begin{aligned}&\left|\psi^{(\alpha)}_{\epsilon,\delta}(r>b)\right\rangle\\&=\frac{1}{r}\left\{\left[f^0_\epsilon(r)-K^0_{oo}g^0_\epsilon(r)\right]|o\rangle-K^0_{co}g^0_{\epsilon-\delta}(r)|c\rangle\right\},\end{aligned} \tag{23}$$

$$\begin{aligned}&\left|\psi^{(\beta)}_{\epsilon,\delta}(r>b)\right\rangle\\&=\frac{1}{r}\left\{-K^0_{oc}g^0_\epsilon(r)|o\rangle+\left[f^0_{\epsilon-\delta}(r)-K^0_{cc}g^0_{\epsilon-\delta}(r)\right]|c\rangle\right\}.\end{aligned} \tag{24}$$

Here the parameter K^0_{ij} $(i,j=o,c)$ is also determined by the detail of the potential curves $U^{(\pm)}(r)$ in the region $r<b$. As shown in Appendix A, with an analysis that is similar to that in Sec. II A, we can find that for our case with $\epsilon\ll\hbar^2/m\beta_6^2$ and $\delta\ll\hbar^2/m\beta_6^2$, the values of K^0_{ij} $(i,j=o,c)$ are independent of both ϵ and δ [18]. Therefore, we can obtain the values of K^0_{ij} $(i,j=o,c)$ from the behavior of $|\psi^{(\alpha,\beta)}_{\epsilon,\delta}(r)\rangle$ in the limit $\delta\to 0$ with the following analysis. In Sec. II A we already obtained two special solutions $|\psi^{(\pm)}_{\epsilon,\delta=0}(r)\rangle$ for Eqs. (9) and (10) with $\delta=0$. Therefore, $|\psi^{(\alpha,\beta)}_{\epsilon,\delta=0}(r)\rangle$ should be the linear combinations of $|\psi^{(\pm)}_{\epsilon,\delta=0}(r)\rangle$. This fact and Eqs. (12), (13), (16), (23), and (24) yield that

$$K^0_{cc}=K^0_{oo}=\tfrac{1}{2}(K^0_++K^0_-), \tag{25}$$

$$K^0_{co}=K^0_{oc}=\tfrac{1}{2}(K^0_--K^0_+). \tag{26}$$

Moreover, with the relation (20) the parameters K^0_{ij} $(i,j=o,c)$ can be further expressed as functions of β_6 and the scattering length $a_s^{(\pm)}$.

C. Scattering wave function and phase shift

Now we calculate the scattering wave function $|\psi_{\epsilon,\delta}(r)\rangle$ that satisfies Eq. (9) as well as both of the boundary conditions (10) and (11). This scattering state is the superposition of the two special solutions $|\psi^{(\alpha,\beta)}_{\epsilon,\delta}(r)\rangle$ of Eqs. (9) and (10), which were derived in Sec. II B. Namely, $|\psi_{\epsilon,\delta}(r)\rangle$ can be expressed as

$$|\psi_{\epsilon,\delta}(r)\rangle=B\left\{\left|\psi^{(\alpha)}_{\epsilon,\delta}(r)\right\rangle+C\left|\psi^{(\beta)}_{\epsilon,\delta}(r)\right\rangle\right\}, \tag{27}$$

where the coefficient C is determined by the condition (11) and the coefficient B could be an arbitrary r-independent constant. In addition, according to this result and Eqs. (23) and (24), in the region $r>b$ the component $\langle c|\psi_{\epsilon,\delta}(r)\rangle$ is a linear combination of functions $f^0_{\epsilon-\delta}(r)$ and $g^0_{\epsilon-\delta}(r)$. In our system with $\epsilon<\delta$, these two functions have asymptotic behaviors [21]

$$\begin{aligned}f^0_{\epsilon-\delta}(r\to\infty)=r^{1/2}\lim_{r\to\infty}\Big[&W_{fI}(\epsilon-\delta)I_{2\nu}(\kappa r)\\&+W_{fK}(\epsilon-\delta)\frac{1}{\pi}K_{2\nu}(\kappa r)\Big],\end{aligned} \tag{28}$$

$$\begin{aligned}g^0_{\epsilon-\delta}(r\to\infty)=r^{1/2}\lim_{r\to\infty}\Big[&W_{gI}(\epsilon-\delta)I_{2\nu}(\kappa r)\\&+W_{gK}(\epsilon-\delta)\frac{1}{\pi}K_{2\nu}(\kappa r)\Big],\end{aligned} \tag{29}$$

where

$$\kappa=\frac{\sqrt{m(\delta-\epsilon)}}{\hbar},$$

$I_{2\nu}$ and $K_{2\nu}$ are Bessel functions, and the functions $W_{ij}(z)$ $(i=f,g;\ j=I,K)$ are defined in in Ref. [21]. Here the ν is a parameter that is determined by the energy $\epsilon-\delta$, as described in Ref. [21]. Substituting Eqs. (28) and (29) into Eq. (27), we can express $\lim_{r\to\infty}\langle c|\psi_{\epsilon,\delta}(r)\rangle$ in terms of the parameter C. Moreover, matching this expression with the boundary condition (11) and using the facts $I_{2\nu}[(\kappa r)\to\infty]=\infty$ and $K_{2\nu}[(\kappa r)\to\infty]=0$, we find that

$$C=\frac{K_{co}W_{gI}(\epsilon-\delta)}{W_{fI}(\epsilon-\delta)-K_{cc}W_{gI}(\epsilon-\delta)}.$$

Substituting this expression into Eq. (27), we obtain the component of the scattering wave function $|\psi_{\epsilon,\delta}(r)\rangle$ in the open channel

$$\langle o|\psi_{\epsilon,\delta}(r>b)\rangle=\frac{B}{r}\left\{f^0_\epsilon(r)-K_{\rm eff}[\epsilon,\delta]g^0_\epsilon(r)\right\}, \tag{30}$$

where the function $K_{\rm eff}[\epsilon,\delta]$ is defined as

$$K_{\rm eff}[\epsilon,\delta]=K^0_{oo}+\frac{K^0_{oc}K^0_{co}}{\chi(\epsilon-\delta)-K^0_{cc}}. \tag{31}$$

Here K^0_{ij} $(i,j=o,c)$ are given in Eqs. (25) and (26), with $K^0_\pm$ being given in Eq. (20), and the function $\chi(z)$ $(z<0)$ is

defined as

$$\chi(z) = \frac{W_{fI}(z)}{W_{gI}(z)}. \tag{32}$$

Substituting Eqs. (17) and (18) into Eq. (30), we can further obtain the behavior of $\langle o|\psi_{\epsilon,\delta}(r)\rangle$ in the limit $r \to \infty$. Comparing this expression with the relation

$$\lim_{r\to 0}\langle o|\psi_{\epsilon,\delta}(r)\rangle \propto \frac{1}{r}[\cot\eta_0(k)\sin(kr) + \cos(kr)], \tag{33}$$

where η_0 is the s-wave scattering phase shift, we finally find that $\cot\eta_0(k)$ can be expressed as

$$\cot\eta_0(k) = \frac{Z_{ff}(\epsilon) - K_{\rm eff}[\epsilon,\delta]Z_{gf}(\epsilon)}{K_{\rm eff}[\epsilon,\delta]Z_{gg}(\epsilon) - Z_{fg}(\epsilon)}. \tag{34}$$

Moreover, since $K_{\rm eff}[\epsilon,\delta]$ is determined by the parameters $K_{ij}^{(0)}$ $(i,j = o,c)$ and $K_{ij}^{(0)}$ is a function of the scattering lengths $a_s^{(\pm)}$ and the characteristic length β_6 of the van der Waals interaction potential, $\tan\eta_0(k)$ given by Eq. (34) is essentially a function of $a_s^{(\pm)}$, β_6, δ, and ϵ. Here we point out that the expression (34) of $\cot\eta_0(k)$ has the same form as the one for the case with a single-channel van der Waals potential (i.e., Eq. (5) of Ref. [17]), while the parameter K_0 for the single-channel case should be replaced by $K_{\rm eff}[\epsilon,\delta]$ for our case.

D. The s-wave scattering length and effective range

Using Eq. (34), we can calculate the two-atom s-wave scattering length a_s and effective range $r_{\rm eff}$, which are defined via the low-energy expansion of $k\cot\eta_0(k)$:

$$k\cot\eta_0(k) = -\frac{1}{a_s} + \frac{1}{2}r_{\rm eff}k^2 + O(k^3). \tag{35}$$

Substituting Eq. (34) into Eq. (35) and using direct calculations that are quite similar to the single-channel case [17], we can obtain

$$a_s(\delta) = \frac{2\pi}{[\Gamma(1/4)]^2}\frac{K_{\rm eff}[0,\delta]-1}{K_{\rm eff}[0,\delta]}\beta_6, \tag{36}$$

$$r_{\rm eff}(\delta) = \frac{[\Gamma(1/4)]^2}{3\pi}\frac{K_{\rm eff}[0,\delta]^2+1}{(K_{\rm eff}[0,\delta]-1)^2}\beta_6 + \frac{[\Gamma(1/4)]^2}{\pi}\frac{\hbar^2 K'_{\rm eff}[0,\delta]}{m\beta_6(K_{\rm eff}[0,\delta]-1)^2}, \tag{37}$$

where $K'_{\rm eff}[\epsilon,\delta] = dK_{\rm eff}[\epsilon,\delta]/d\epsilon$. In addition, with the help of the relation $\delta = (\delta\mu)B$, we can further express a_s and $r_{\rm eff}$ as functions of the magnetic field B. It is clear that we have $a_s = \infty$ at the magnetic field B_0, which satisfies the condition

$$K_{\rm eff}[0,(\delta\mu B_0)] = 0. \tag{38}$$

That is the OFR.

In the calculation for a_s and $r_{\rm eff}$ we are required to derive the value of the function $\chi(-\delta)$, which appears in the expression (31) for $K_{\rm eff}[0,\delta]$. The exact value of $\chi(-\delta)$ can be obtained from its definition (32) and the expressions of the W functions that are given in Ref. [21]. Nevertheless, it is also proved that [19] for sufficient small $|z|$ the expression of $\chi(z)$ $(z<0)$ can be approximated as [see Eq. (57) of [19]; notice that the function $\chi_{l=0}^{c0}$ in this reference means $-\chi$ for our case]

$$\chi(z) \approx \frac{\frac{\tilde z}{3} + \frac{\pi\tilde z^2}{30} - \frac{2\pi\sqrt{\tilde z}\left(1+\frac{\tilde z}{3}\right)}{\Gamma[1/4]^2}}{1 - \frac{2\pi\sqrt{\tilde z}\left(1-\frac{\tilde z}{3}\right)}{\Gamma[1/4]^2}}, \tag{39}$$

with $\tilde z = |z|m\beta_6^2/\hbar^2$. Therefore, when the energy gap δ is small enough (i.e., the magnetic field B is small enough) we can use the approximation (39) to simplify the calculations for a_s and $r_{\rm eff}$. Similarly, according to Eq. (28) of Ref. [19] (notice that K_l^{c0} in that reference means $-K_{\rm eff}$ for our case), when both δ and the scattering energy ϵ are small enough, the expression (34) of $\cot\eta_0$ can be approximated as

$$\cot\eta_0 \approx \left[\frac{\pi\tilde k^4}{15} - \frac{2\pi\tilde k}{\Gamma\left[\frac{1}{4}\right]^2}\frac{1-\tilde K-(1+\tilde K)\left(\frac{1}{3}\tilde k^2+\frac{\pi}{30}\tilde k^4\right)}{-\tilde K-\frac{1}{3}\tilde k^2+\frac{\pi}{30}\tilde k^4}\right]^{-1} \times\left[1 - \frac{4\tilde k^4}{15}\ln\tilde k + \frac{2}{15}\left(\frac{22}{5}+\ln 2-\gamma\right)\tilde k^4\right]^{-1}, \tag{40}$$

where $\tilde k = k\beta_6$, $\gamma = 0.5772\ldots$ is the Euler constant and $\tilde K$ is the value of $K_{\rm eff}[\epsilon,\delta]$ given by Eq. (31), with the value of $\chi(\epsilon-\delta)$ given by the approximation (39).

In Fig. 3 we illustrate the scattering length a_s for ^{173}Yb with $a_s^{(+)} = 1900a_0$, $a_s^{(-)} = 200a_0$ [5], and $\beta_6 = 169.6a_0$ [15], with a_0 the Bohr radius. Here we consider the case with $m_I = -5/2$ and $m'_I = 5/2$. We calculate a_s with both the exact value of the function $\chi(-\delta)$ and the approximation (39). It is shown that the approximation (39) works very well for $B \lesssim 60$ G.

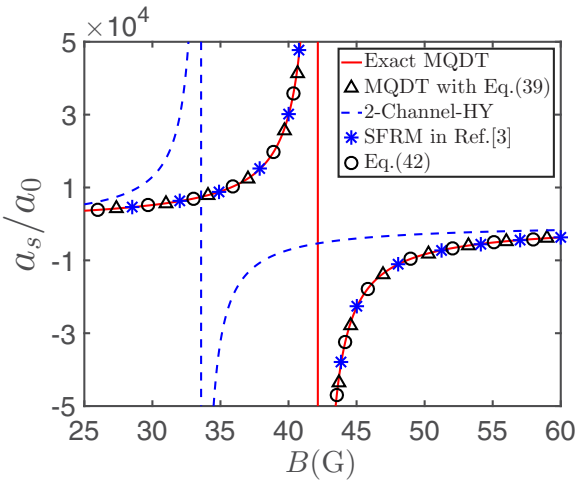

FIG. 3. The s-wave scattering length a_s of ^{173}Yb atoms, as a function of magnetic field. Here we show the results given by the MQDT [i.e., Eq. (36)] with the exact value of $\chi(-\delta)$ (red solid line), the MQDT with the approximation (39) (black triangle), the two-channel Huang-Yang (HY) pseudopotential [i.e., Eq. (41)] (blue dashed line), the approximated expression (42) (black circles), and the simple finite-range model (SFRM) in Ref. [3] (blue stars). We consider the case with $m_I = -5/2$ and $m'_I = 5/2$ and take $a_s^{(+)} = 1900a_0$, $a_s^{(-)} = 200a_0$, $\beta_6 = 169.6a_0$ with a_0 the Bohr radius, and $\mu_e - \mu_g = 2\pi\hbar \times 112$ Hz/G. The results of the SFRM are given by Eq. (12) of Ref. [3] with the parameter $r_0 = 112.9a_0$.

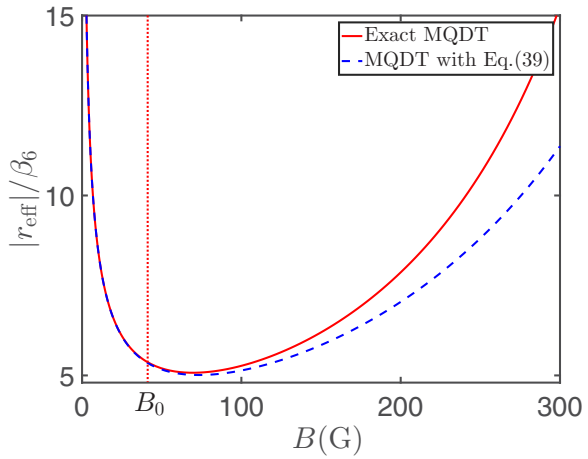

FIG. 4. Effective range $r_{\rm eff}$ of ^{173}Yb atoms given by the MQDT with the exact value of $\chi(-\delta)$ (red solid line) and the MQDT with the approximation (39) (blue dashed line). The red dotted line indicates the OFR point B_0. In our calculation we use the same parameters as in Fig. 3.

For comparison, we also show a_s given by the zero-range two-channel Huang-Yang pseudopotential, which can be expressed as [3,16]

$$a_s = \frac{-[a_s^{(+)} + a_s^{(-)}] + 2\sqrt{m\delta/\hbar^2}\, a_s^{(+)} a_s^{(-)}}{[a_s^{(+)} + a_s^{(-)}]\sqrt{m\delta/\hbar^2} - 1}. \tag{41}$$

As show in Fig. 3, the difference between the OFR points given by the MQDT and the zero-range two-channel Huang-Yang pseudopotential is about 9 G and the relative difference is about 20%. This difference is due to the fact that the zero-range pseudopotential does not include the van der Waals physics and thus is less accurate than the MQDT approach. In Fig. 3 we also compare the result given by the MQDT and the one given by the simple finite-range model (SFRM) in Ref. [3] (i.e., Eq. (12) of Ref. [3]), where the interaction potential is simply described by a finite-range boundary condition satisfied by the wave function at the position $r = r_0$. It is shown that for our case the SFRM is quantitatively consistent with the MQDT when $r_0 = 112.9a_0 \approx 0.67\beta_6$.

On the other hand, around the OFR point B_0 where $a_s = \infty$, we can expand the scattering length a_s as a series of $B - B_0$. By neglecting the high-order terms that are proportional to $(B - B_0)^n$ $(n \geqslant 1)$, we obtain the approximate expression of a_s:

$$a_s \approx a_{\rm bg}\left(1 - \frac{\Delta_B}{B - B_0}\right). \tag{42}$$

Our calculation show that for ^{173}Yb we have $a_{\rm bg} = -98a_0$ and $\Delta_B = -660$ G. As shown in Fig. 3, this approximate expression is quantitatively consistent with the MQDT result [i.e., Eq. (36)] in a large range of magnetic field.

In Fig. 4 we illustrate the effective range $r_{\rm eff}$ for the OFR of ^{173}Yb atoms with $m_I = -5/2$ and $m_I' = 5/2$. Our calculation shows that at the OFR point we have $|r_{\rm eff}| \approx 908.7a_0 \approx 5.4\beta_6$ and thus the resonance parameter $s_{\rm res} \equiv 4\pi\beta_6/\,\Gamma(1/4)^2 r_{\rm eff}$ is about 0.18. This means that OFR for ^{173}Yb is a narrow resonance in the sense of an effective range [2,7]. Here we also

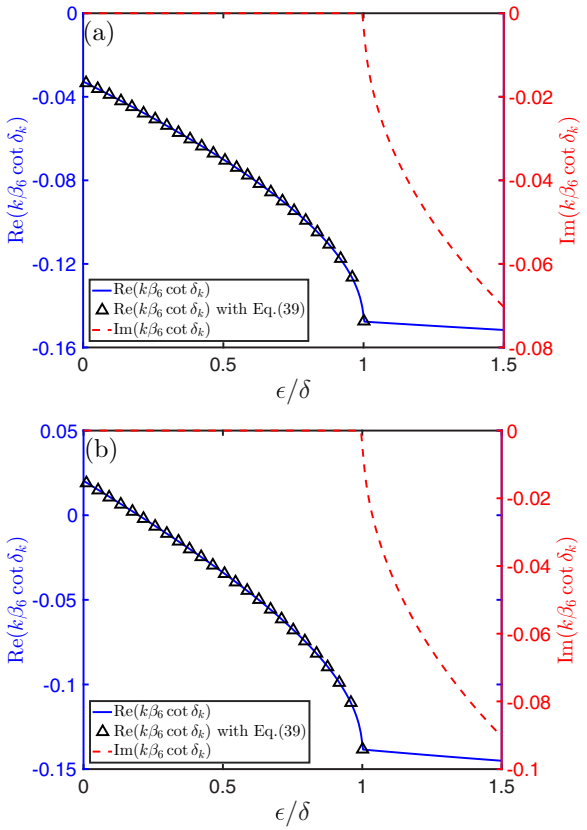

FIG. 5. Real part (blue solid line) and imaginary part (red dashed line) of the factor $k\cot\eta_0$ defined by Eq. (33), as functions of the scattering energy ϵ. Here we consider the system with the parameters of Fig. 3 and illustrate the results for the cases with (a) $B = 30$ G ($\delta = 2\pi\hbar \times 1.7 \times 10^4$ Hz) and (b) $B = 50$ G ($\delta = 2\pi\hbar \times 2.8 \times 10^4$ Hz). It is clearly shown that $\mathrm{Im}[k\cot\eta_0] = 0$ for $\epsilon < \delta$ and $\mathrm{Im}[k\cot\eta_0] \neq 0$ for $\epsilon > \delta$. The black triangles are the results for $\mathrm{Re}[k\cot\eta_0]$ $(\epsilon < \delta)$ given by the approximation (40). Our calculation for the case with $\epsilon > \delta$ is based on the boundary condition $\lim_{r\to\infty}\langle c|\psi_{\epsilon,\delta}(r)\rangle \propto e^{i\sqrt{m(\epsilon-\delta)}r/\hbar}/r$ and the direct generalization of the approach in Secs. II A–II C for that case.

compare the results given by the exact value of the function $\chi(-\delta)$ and the approximation (39) and show that an apparent difference between these two results appears for $B \gtrsim 100$ G.

It is pointed out that the effective range diverges in the limit $B \to 0$, as shown in Fig. 4. That is due to the fact that the function $\frac{d\chi(z)}{dz}|_{z=-\delta}$, which is proportional to $K'[0,\delta]$, diverges in the limit $\delta \to 0$. This result may also be understood with the following analysis. We consider the scattering of two atoms incident from the channel $|o\rangle$. When the scattering energy ϵ is smaller than the energy gap δ between channels $|c\rangle$ and $|o\rangle$, the channel $|o\rangle$ is open and $|c\rangle$ is closed. Thus, there is only elastic scattering $|o\rangle \to |o\rangle$. Accordingly, the parameter $k\cot\eta_0$ defined by Eq. (33) is real. Nevertheless, when $\epsilon > \delta$, both channels $|o\rangle$ and $|c\rangle$ are open. As a result, there are both elastic scattering $|o\rangle \to |o\rangle$ and inelastic scattering $|o\rangle \to |c\rangle$. Thus, the boundary condition (11) should be replaced by $\lim_{r\to\infty}\langle c|\psi_{\epsilon,\delta}(r)\rangle \propto e^{i\sqrt{m(\epsilon-\delta)}r/\hbar}/r$, which includes both real and imaginary parts. As a result, the imaginary part of $k\cot\eta_0$ becomes nonzero, as illustrated in Fig. 5. Therefore,

as a function of k, the factor $k\cot\eta_0$ is not analytical at the point $k=\sqrt{\delta}$. As a result, when $\delta=0$ (i.e., $B=0$) the factor $k\cot\eta_0$ is not analytical at $k=0$ and thus the effective-range expansion (35) is not applicable for finite k. Accordingly, the expansion coefficient $r_{\rm eff}$ diverges in the limit $B\to 0$.

III. TWO-ATOM BOUND STATE

In this section we investigate the two-atom bound state in the system with OFR. We will calculate the binding energy and wave function with MQDT and study the clock-transition spectrum for the bound state, which may be observed in the experiments.

A. Binding energy and wave function

In our system the two-body bound-state wave function $|\phi_b(r)\rangle$ and the bound-state energy E_b satisfy the Schrödinger equation

$$\hat{H}|\phi_b(r)\rangle = E_b|\phi_b(r)\rangle \tag{43}$$

as well as the conditions

$$\lim_{r\to 0}(r|\phi_b(r)\rangle)=0, \tag{44}$$

$$\lim_{r\to\infty}|\phi_b(r)\rangle=0, \tag{45}$$

and

$$E_b<0. \tag{46}$$

Here we consider the cases where the binding energy $|E_b|$ is much smaller than $\hbar^2/m\beta_6^2$. In these cases we can derive E_b with the MQDT approach introduced above. With the analysis shown in the above section, we can obtain two special solutions $|\psi^{(\alpha)}_{E_b,\delta}(r)\rangle$ and $|\psi^{(\beta)}_{E_b,\delta}(r)\rangle$ for Eqs. (43) and (44). In the region $r>b$, the solutions $|\psi^{(\alpha,\beta)}_{E_b,\delta}(r)\rangle$ also satisfy Eqs. (23) and (24) with K^0_{ij} $(i,j=o,c)$ being given by Eqs. (25) and (26) and $\epsilon=E_b$. The bound-state wave function $|\phi_b(r)\rangle$ can be expressed as the superposition of these two special solutions, i.e., we have

$$|\phi_b(r)\rangle = C_\alpha\left|\psi^{(\alpha)}_{E_b,\delta}(r)\right\rangle + C_\beta\left|\psi^{(\beta)}_{E_b,\delta}(r)\right\rangle, \tag{47}$$

with $C_{\alpha,\beta}$ the superposition coefficients. Furthermore, substituting the behaviors of the functions $f^{(0)}_\epsilon(r)$ and $g^{(0)}_\epsilon(r)$ in the long-range limit $r\to\infty$, i.e., Eqs. (26) and (27) of Ref. [21], we can derive the long-range behavior of the special solutions $|\psi^{(\alpha,\beta)}_{E_b,\delta}(r)\rangle$. Substituting this behavior into the expression (47) and then into the boundary conditions (44) and (45), we can finally derive the algebraic equation satisfied by the bound-state energy E_b,

$$\chi(E_b)=K_{\rm eff}[E_b,\delta], \tag{48}$$

with the function $\chi(z)$ and $K_{\rm eff}[z,\delta]$ introduced in Sec. II C. We can obtain the energy E_b by solving Eq. (48).

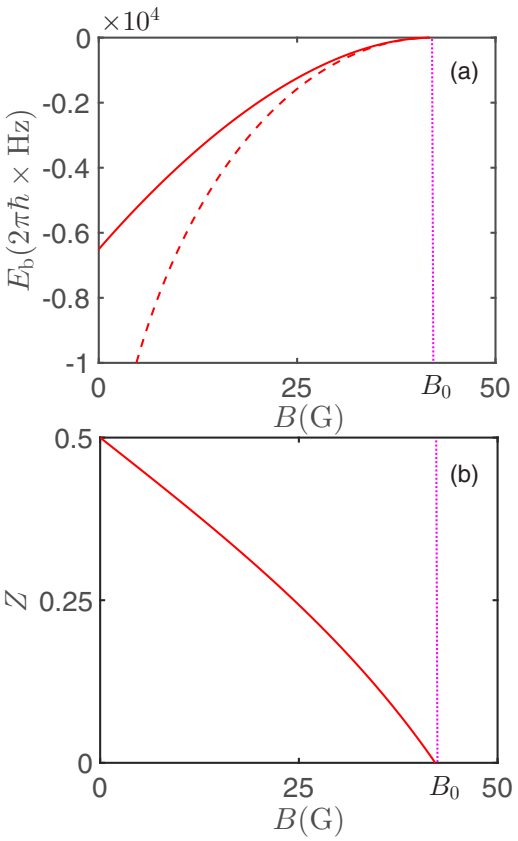

FIG. 6. (a) Bound-state energy E_b and (b) closed-channel population Z of ^{173}Yb atoms. Here we show the value of E_b given by the MQDT (red solid line) and the simple expression $E_s\equiv-\hbar^2/ma_s^2$ (red dashed line). In our calculation we use the same parameters as in Fig. 3. Here the pink dotted line indicates the OFR point B_0.

Furthermore, we can also calculate the closed-channel population Z of the two-body bound state, which is defined as

$$Z\equiv\frac{\int|\langle c|\phi_b(r)\rangle|^2d\mathbf{r}}{\int[|\langle c|\phi_b(r)\rangle|^2+|\langle o|\phi_b(r)\rangle|^2]d\mathbf{r}}. \tag{49}$$

Using the Feynman-Hellmann theorem, it can be proved that the value of Z is given by the derivative of the bound-state energy E_b with respect to the energy gap δ between the open and closed channels:

$$Z=\frac{\partial E_b}{\partial\delta}. \tag{50}$$

In Figs. 6(a) and 6(b) we illustrate the bound-state energy E_b and the closed-channel population Z for ^{173}Yb atoms, as functions of the magnetic field B. For comparison, we also show the energy given by the simple expression $E_s\equiv-\hbar^2/ma_s^2$, with a_s the s-wave scattering length given by the MQDT. For a wide Feshbach resonance that is dominated by the open channel, we have $E_b\approx E_s$ and $Z\approx 0$ in a broad region around the resonance point. Nevertheless, as shown in Figs. 6(a) and 6(b), in most of the resonance region of ^{173}Yb atoms the behaviors of E_b and E_s are quite different from each other and the closed-channel population Z is significantly

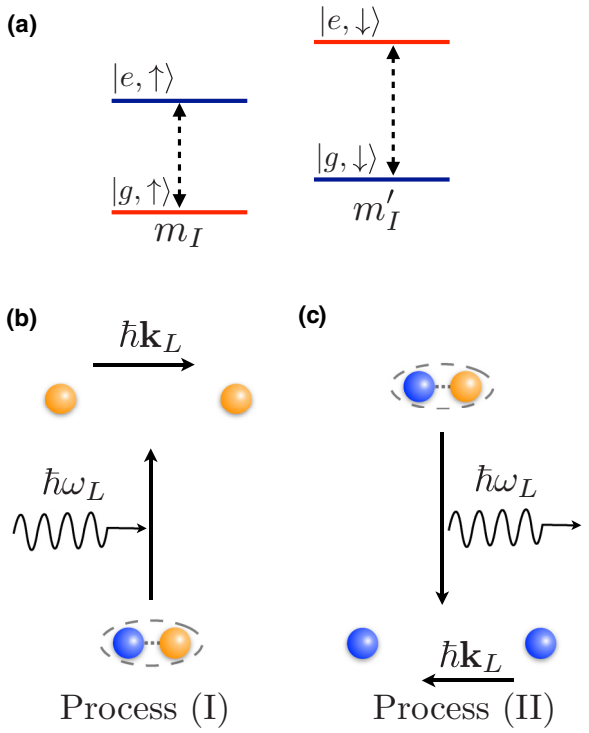

FIG. 7. (a) Schematic diagram for the experiment of clock-transition spectrum. The π-polarized clock laser can induce a one-body transition between states $|g,\uparrow\rangle$ and $|e,\uparrow\rangle$, as well as the transition between $|g,\downarrow\rangle$ and $|e,\downarrow\rangle$. As defined in Sec. II, m_I and m_I' are the magnetic quantum numbers for the nuclear spin states $\uparrow$ and $\downarrow$, respectively. (b) and (c) Two processes of clock-laser-induced dissociation of a dimer, where one atom (the yellow atom) is in the e state and the other atom (the blue atom) is in the g state. Process (I): The atom in the g state absorbs a photon and transits to the e state. The two-atom mass center gains photon recoil momentum $\hbar\mathbf{k}_L$. Process (II): The atom in the e state emits a photon and transits to the g state. The two-atom mass center gains photon recoil momentum $-\hbar\mathbf{k}_L$.

nonzero. These results also imply that the OFR for ^{173}Yb is a narrow resonance in which the contribution from the closed channel is quite significant. That is consistent with our previous analysis based on the effective range.

B. Clock-transition spectrum

Now we investigate the clock-transition spectrum for the ultracold gases of alkali-earth-metal-like atoms in the two-body bound state $|\phi_b(r)\rangle$ (i.e., the ultracold gases of dimers). It is clear that in each dimer one atom is in the electronic orbital g state and the other atom is in the e state. Therefore, if a pulse of clock laser with π polarization, which can induce the one-body transition (clock transition) between states $|g,j\rangle$ and $|e,j\rangle$ ($j=\uparrow,\downarrow$), is applied to these two atoms, the dimer may be dissociated into two free atoms via the following two first-order processes (Fig. 7).

Process (I). The atom in the g state absorbs a photon and transits to the e state. After this process both of the atoms are in the e state. Since in $|\phi_b(r)\rangle$ one atom is in nuclear-spin state $\uparrow$ and the other atom is in state $\downarrow$ and the π-laser beam does not change the nuclear-spin state, after this process we have one atom in state $|e,\uparrow\rangle$ and the other atom in state $|e,\downarrow\rangle$. Furthermore, the center of mass (c.m.) of these two atoms can obtain a recoil momentum $\hbar\mathbf{k}_\mathrm{L}$ from the laser photon, with $\mathbf{k}_\mathrm{L}$ being the wave vector of the clock laser.

Process (II). The atom in the e state emits a photon and transits to the g state. With similar analysis, we know that after this process one atom is in state $|g,\uparrow\rangle$ and the other atom is in state $|g,\downarrow\rangle$ and the c.m. can also obtain a recoil momentum $-\hbar\mathbf{k}_\mathrm{L}$.

Now we study the properties of the clock-transition spectrum, i.e., the dissociation rate as a function of the clock-laser angular frequency ω_L. We first consider the energy condition of the above two processes. Before the transition process, the energy of these two atoms is

$$E_0 = E_{e\uparrow} + E_{g\downarrow} - |E_b| + \frac{\hbar^2|\mathbf{K}|^2}{4m}, \tag{51}$$

where $\hbar\mathbf{K}$ is the c.m. momentum. Here E_{lj} ($l=e,g$; $j=\uparrow,\downarrow$) is the energy of the one-atom internal state $|l,j\rangle$, which can be expressed as $E_{g\uparrow}=\mu_g m_I B$, $E_{g\downarrow}=\mu_g(m_I')B$, $E_{e\uparrow}=\epsilon_{eg}+\mu_e m_I B$, and $E_{e\downarrow}=\epsilon_{eg}+\mu_e(m_I')B$, with ϵ_{eg} the energy gap between the e state and g state for $B=0$. The term $E_{e\uparrow}+E_{g\downarrow}$ in Eq. (51) is nothing but the threshold energy of the open channel $|o\rangle$. Now we consider process (I) in which the atoms absorb a photon. Due to the energy conservation, this process can occur under the condition

$$E_0 + \hbar\omega_\mathrm{L} > E_\mathrm{min}^{(\mathrm{I})}, \tag{52}$$

where $E_\mathrm{min}^{(\mathrm{I})}$ is the minimum energy of the final states of process (I). Furthermore, since the finial state of process (I) is a scattering state of two atoms in states $|e,\uparrow\rangle$ and $|e,\downarrow\rangle$, with mass-center momentum $\hbar(\mathbf{K}+\mathbf{k}_\mathrm{L})$, the minimum energy of the final state of process (I) is

$$E_\mathrm{min}^{(\mathrm{I})} = E_{e\uparrow} + E_{e\downarrow} + \frac{\hbar^2|\mathbf{K}+\mathbf{k}_\mathrm{L}|^2}{4m}. \tag{53}$$

Thus, the energy condition (52) for process (I) can be rewritten as

$$\omega_\mathrm{L} > \omega_\mathrm{I}(\mathbf{K}) \equiv \frac{E_{e\downarrow} - E_{g\downarrow} + |E_b|}{\hbar} + \frac{\hbar(|\mathbf{k}_\mathrm{L}|^2 + 2\mathbf{K}\cdot\mathbf{k}_\mathrm{L})}{4m}. \tag{54}$$

Similarly, since in process (II) the atoms emit a photon, this process can occur under the condition

$$E_0 - \hbar\omega_\mathrm{L} > E_\mathrm{min}^{(\mathrm{II})}, \tag{55}$$

where $E_\mathrm{min}^{(\mathrm{II})}$ is the minimum energy of the final states of process (II), which can be expressed as

$$E_\mathrm{min}^{(\mathrm{II})} = E_{g\uparrow} + E_{g\downarrow} + \frac{\hbar^2|\mathbf{K}-\mathbf{k}_\mathrm{L}|^2}{4m}. \tag{56}$$

Using this result, we can reexpress the energy condition (55) for process (II) as

$$\omega_\mathrm{L} < \omega_\mathrm{II}(\mathbf{K}) \equiv \frac{E_{e\uparrow} - E_{g\uparrow} - |E_b|}{\hbar} - \frac{\hbar(|\mathbf{k}_\mathrm{L}|^2 - 2\mathbf{K}\cdot\mathbf{k}_\mathrm{L})}{4m}. \tag{57}$$

The above analysis yields that the laser-induced dissociation process can only occur under the condition (54) or (57).

In particular, the dissociation process cannot occur in the frequency region $\omega_{\rm II} < \omega < \omega_{\rm I}$. Thus, the clock-transition spectrum includes two branches corresponding to processes (I) and (II), respectively.

Our above analysis can be verified by the quantitative calculation for the dissociation rate based on Fermi's golden rule. We consider two atoms with the initial wave function

$$|\Psi(\mathbf{R},\mathbf{r},t=0)\rangle = \frac{1}{(2\pi)^{3/2}}\int d\mathbf{K}\,\phi(\mathbf{K})e^{i\mathbf{K}\cdot\mathbf{R}}|\phi_b(r)\rangle, \quad (58)$$

where $\mathbf{R}$ and $\mathbf{r}$ are the mass-center position and the relative position of these two atoms, respectively, $|\phi_b(r)\rangle$ is the two-atom bound-state wave function we obtained in the preceding section, and $\phi(\mathbf{K})$ is the wave function of the c.m. motion in the momentum space. We further assume that the laser beam is applied from the time $t = 0$.

At time t the probability of the two atoms being in the bound state can be denoted by $P(t)$. Fermi's golden rule yields that (Appendix B) when t is short we have [24]

$$P(t) \approx 1 - \Gamma t. \quad (59)$$

Here Γ is the dissociation rate. Furthermore, as shown in Appendix B, for our system it can be proved that

$$\Gamma = \int d\mathbf{K}|\phi(\mathbf{K})|^2\gamma(\mathbf{K}), \quad (60)$$

where $\gamma(\mathbf{K})$ is the dissociation rate corresponding to the mass-center momentum $\hbar\mathbf{K}$, which can be expressed as

$$\gamma(\mathbf{K}) = \gamma_{\rm I}(\mathbf{K}) + \gamma_{\rm II}(\mathbf{K}). \quad (61)$$

Here $\gamma_l(\mathbf{K})$ ($l = {\rm I,II}$) is the dissociate rate for process l and is given by

$$\gamma_l(\mathbf{K}) = \frac{\pi}{\hbar}\sum_{j=1,2}\int d\mathbf{k}\left|\int d\mathbf{r}\langle\Psi_j^l(\mathbf{k},\mathbf{r})|\Lambda(\mathbf{r})|\phi_b(r)\rangle\right|^2 \times \delta\left(\hbar\omega_l(\mathbf{K}) + \xi_l\frac{\hbar^2|\mathbf{k}|^2}{2m} - \hbar\omega_{\rm L}\right), \quad (62)$$

with $\xi_{\rm I} = 1$, $\xi_{\rm II} = -1$, and $\omega_{\rm I,II}(\mathbf{K})$ defined in Eqs. (54) and (57). Here the operator $\Lambda(\mathbf{r})$ is defined as $\Lambda(\mathbf{r}) = \frac{\hbar\Omega}{2}(|e\rangle^{(1)}\langle g|e^{i\mathbf{k}_{\rm L}\cdot\mathbf{r}/2} + |e\rangle^{(2)}\langle g|e^{-i\mathbf{k}_{\rm L}\cdot\mathbf{r}/2}) + {\rm H.c.}$, where Ω is the Rabi frequency of the laser. In Eq. (62) $|\Psi_j^l(\mathbf{k},\mathbf{r})\rangle$ ($l = {\rm I,II}$; $j = 1,2$) is the final state of process l, i.e., the scattering wave functions of two atoms with incident momentum $\mathbf{k}$ and two-atom internal states

$$|{\rm I},1\rangle \equiv \frac{1}{\sqrt{2}}|e\rangle^{(1)}|e\rangle^{(2)}[|\uparrow\rangle^{(1)}|\downarrow\rangle^{(2)} + |\downarrow\rangle^{(1)}|\uparrow\rangle^{(2)}], \quad (63)$$

$$|{\rm I},2\rangle \equiv \frac{1}{\sqrt{2}}|e\rangle^{(1)}|e\rangle^{(2)}[|\uparrow\rangle^{(1)}|\downarrow\rangle^{(2)} - |\downarrow\rangle^{(1)}|\uparrow\rangle^{(2)}], \quad (64)$$

$$|{\rm II},1\rangle \equiv \frac{1}{\sqrt{2}}|g\rangle^{(1)}|g\rangle^{(2)}[|\uparrow\rangle^{(1)}|\downarrow\rangle^{(2)} + |\downarrow\rangle^{(1)}|\uparrow\rangle^{(2)}], \quad (65)$$

$$|{\rm II},2\rangle \equiv \frac{1}{\sqrt{2}}|g\rangle^{(1)}|g\rangle^{(2)}[|\uparrow\rangle^{(1)}|\downarrow\rangle^{(2)} - |\downarrow\rangle^{(1)}|\uparrow\rangle^{(2)}]. \quad (66)$$

Notice that we have $\langle l,j|o\rangle = \langle l,j|c\rangle = 0$ for $l = {\rm I,II}$ and $j = 1,2$. Thus, $|\Psi_j^l(\mathbf{k},\mathbf{r})\rangle$ are orthogonal to the initial two-body bound state $|\phi_b(r)\rangle$.

Furthermore, Eq. (60) implies that if the mass-center momentum is mainly distributed in a small region around a central momentum $\mathbf{K}_0$, we have $\Gamma \approx \gamma(\mathbf{K}_0)$. In the following we consider the simple case with $\mathbf{K}_0 = \mathbf{0}$. We further calculate $\gamma(\mathbf{0})$ for ^{173}Yb atoms for the cases with a different magnetic field. Our calculation is based on the binding energy E_b and the closed-channel population Z derived with the MQDT in Sec. III A. On the other hand, since in our system both E_b and the energy gap δ between the channels $|c\rangle$ and $|o\rangle$ are much smaller than the van der Waals energy, in the bound state $|\phi_b(r)\rangle$ the two-atom relative position r is mainly distributed in the region $r \gtrsim \beta_6$. Thus, in our calculation we ignore the contribution from the two-atom relative function $|\phi_b(r)\rangle$ in the region $r \lesssim \beta_6$ and use the approximated bound-state wave function

$$|\phi_b(r)\rangle = \sqrt{1-Z}\frac{e^{-r/r_o}}{\sqrt{2\pi r_o r}}|o\rangle + \sqrt{Z}\frac{e^{-r/r_c}}{\sqrt{2\pi r_c r}}|c\rangle \quad (67)$$

and the approximated scattering-state wave functions

$$|\Psi_j^l(\mathbf{k},\mathbf{r})\rangle = \frac{(1-P_{12})}{4\pi^{3/2}}\left\{\left[e^{i\mathbf{k}\cdot\mathbf{r}} + \frac{-1}{ik + \frac{1}{a_l}}e^{ikr}\right]|l,j\rangle\right\} \quad (l = {\rm I,II};\ j = 1,2), \quad (68)$$

with states $|l,j\rangle$ being defined in Eqs. (63)–(66). Here we also have $r_o = \hbar/\sqrt{m|E_b|}$, $r_c = \hbar/\sqrt{m(|E_b| + \delta)}$, $a_{\rm I} = a_{ee}$, and $a_{\rm II} = a_{gg}$, where a_{ee} (a_{gg}) is the scattering length of two atoms that are both in the e state (g state). In Eq. (68), P_{12} is the permutation operator for atoms 1 and 2. Explicitly, P_{12} represents the transformations $\mathbf{r} \to -\mathbf{r}$, $|l,1\rangle \to |l,2\rangle$, and $|l,2\rangle \to |l,1\rangle$ for $l = {\rm I,II}$.

In Fig. 8 we show $\gamma(\mathbf{0})$ as a function of $\omega_{\rm L}$ for ^{173}Yb atoms with various magnetic fields. It is clear that for each magnetic field the clock-transition spectrum has two branches,

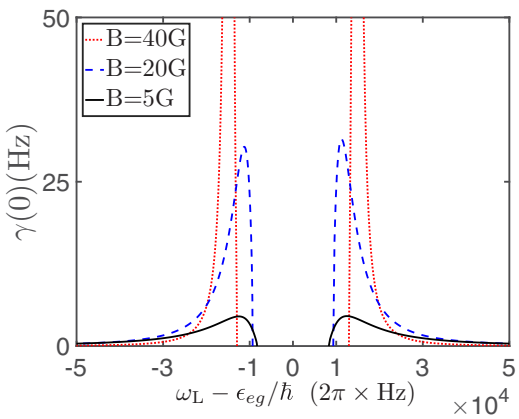

FIG. 8. Clock-transition spectrum for two ^{173}Yb atoms in the bound state $|\phi_b(r)\rangle$ with $B = 5$ G [$|E_b| = \hbar \times (2\pi)5176.05$ Hz, black solid line], $B = 20$ G [$|E_b| = \hbar \times (2\pi)2007.59$ Hz, blue dashed line], and $B = 40$ G [$|E_b| = \hbar \times (2\pi)22.63$ Hz, red dotted line]. In our calculation we take $m_I = -5/2$, $m_I' = 5/2$, $\Omega = (2\pi)10^3$ Hz, $\epsilon_{eg} = \hbar \times (2\pi)5.19 \times 10^{14}$ Hz [25,26], $a_{gg} = 199.4a_0$, $a_{ee} = 306.2a_0$ [15], and $\mu_e - \mu_g = \hbar \times (2\pi)112$ Hz/G. The maximum value of $\gamma(\mathbf{0})$ for $B = 40$ G is 772 Hz. For a given magnetic field, the right and left branches of the spectrum correspond to transition processes (I) and (II), respectively.

corresponding to process (I) (right branch with $\omega_L > \omega_I$) and process (II) (left branch with $\omega_L < \omega_{II}$), as we have analyzed before. Furthermore, it is also shown that when the magnetic field is close to the OFR point B_0, the spectrum becomes sharper. This result may be explained as follows. When the system is close to the OFR point, the wave packet of the bound state becomes very wide in the real space and thus very narrow in the momentum space. Therefore, in this case the bound state has significant overlap (the Frank-Condon factor) only with the scattering states $|\Psi_j^l(\mathbf{k},\mathbf{r})\rangle$ with incident momentum and scattering energy being in a small region and thus the transition spectrum becomes narrow.

Our above results, together with Eqs. (54) and (57), show that both the position and the shape of the clock-transition spectrum are related to the binding energy E_b and the wave function of the two-body bound state $|\phi_b(r)\rangle$. Thus, in the experiments one can detect the properties of $|\phi_b(r)\rangle$ via the clock-transition spectrum.

IV. SUMMARY

In this paper we solve the two-body problem of two alkali-earth-metal-like atoms with OFR via the MQDT approach, in which the effect induced by the van der Waals interaction potential can be analytically included. We derive the analytical expression of the scattering length [Eq. (36)] and the effective range [Eq. (37)], as well as the algebraic equation (48) for the binding energy of the two-body bound state. We further investigate the clock-transition spectrum for our system, which can be used for the experimental detection of the bound state. As in the analysis for the Raman spectrum of ultracold alkali-metal atoms [27–29], here we take into account the momentum recoil effect induced by the clock laser. Since the MQDT approach is quantitatively applicable for the system where all the characteristic energies are much smaller than the van der Waals energy, e.g., the ^{173}Yb atoms near the OFR point, our results are helpful for both theoretical and experimental research for these systems.

ACKNOWLEDGMENTS

We thank Bo Gao and Hui Zhai for helpful discussions. This work was supported by the Natural Science Foundation of China under Grants No. 11434011 and No. 11674393, NKBRSF of China under Grant No. 2012CB922104, the Fundamental Research Funds for the Central Universities, and the Research Funds of Renmin University of China under Grant No. 16XNLQ03.

APPENDIX A: THE ϵ AND δ DEPENDENCES OF K_{ij}^0

In this Appendix we show that the parameters K_{ij}^0 $(i,j = o,c)$ in Sec. II B are independent of ϵ and δ. This fact can be understood with the following analysis, which is quite similar to that in Sec. II A.

First, in the region with $r \lesssim \beta_6$ the interaction potentials $U^{(\pm)}(r)$ are potential wells with the depth being on the order of the van der Waals energy $\hbar^2/m\beta_6^2$ or even larger. Thus, for our case with $\epsilon \ll \hbar^2/m\beta_6^2$ and $\delta \ll \hbar^2/m\beta_6^2$, for $r \lesssim \beta_6$, ϵ and δ can be omitted from the Schrödinger equation (9). Thus, we know that there exist two special solutions of Eq. (9) and the condition (10), which are independent of ϵ and δ for $r \lesssim \beta_6$. We denote these two solutions by $|\Phi_1(r)\rangle$ and $|\Phi_2(r)\rangle$.

Second, since both $|\psi_{\epsilon,\delta}^{(\alpha,\beta)}(r)\rangle$ introduced in Sec. II B and $|\Phi_{1,2}(r)\rangle$ are special solutions of Eqs. (9) and (10), $|\psi_{\epsilon,\delta}^{(\alpha,\beta)}(r)\rangle$ can be expressed as linear superpositions of $|\Phi_{1,2}(r)\rangle$. Namely, we have

$$\left|\psi_{\epsilon,\delta}^{(l)}(r)\right\rangle = \sum_{j=1,2} A_j^{(l)} |\Phi_j(r)\rangle. \tag{A1}$$

Here the coefficients $A_j^{(l)}$ $(l = \alpha,\beta;\ j = 1,2)$ are determined by the following two conditions given by Eqs. (23) and (24). (a) For $b < r \lesssim \beta_6$, if $r\sum_{j=1,2} A_j^{(\alpha)}\langle c|\Phi_j(r)\rangle$ is expanded as a superposition of the functions $f_{\epsilon-\delta}^0(r)$ and $g_{\epsilon-\delta}^0(r)$, then the coefficient for $f_{\epsilon-\delta}^0(r)$ is zero. (b) For $b < r \lesssim \beta_6$, if $r\sum_{j=1,2} A_j^{(\beta)}\langle o|\Phi_j(r)\rangle$ is expanded as a superposition of the functions $f_\epsilon^0(r)$ and $g_\epsilon^0(r)$, then the coefficient for $g_\epsilon^0(r)$ is zero.

Third, as shown above, in the region with $b < r \lesssim \beta_6$ the solutions $|\Phi_{1,2}(r)\rangle$ are independent of ϵ and δ. Furthermore, as illustrated in Fig. 2, for $|\epsilon| \ll \hbar^2/m\beta_6^2$ and $r \lesssim \beta_6$ both $f_\epsilon^0(r)$ and $g_\epsilon^0(r)$ are almost independent of the values of ϵ, for both positive and negative ϵ [21]. Therefore, for our case with $\epsilon \ll \hbar^2/m\beta_6^2$ and $\delta \ll \hbar^2/m\beta_6^2$, in the region with $b < r \lesssim \beta_6$ the functions $f_\epsilon^0(r)$, $g_\epsilon^0(r)$, $f_{\epsilon-\delta}^0(r)$, and $g_{\epsilon-\delta}^0(r)$ are also (ϵ,δ) independent. Thus, the coefficients $A_j^{(l)}$ $(l = \alpha,\beta;\ j = 1,2)$ given by the above conditions (a) and (b) are (ϵ,δ) independent. With this result and Eq. (A1), we know that the functions $|\psi_{\epsilon,\delta}^{(\alpha\beta)}(r)\rangle$ are (ϵ,δ) independent for $b < r \lesssim \beta_6$. Using this fact and Eqs. (23) and (24), as well as the fact that $f_\epsilon^0(r)$, $g_\epsilon^0(r)$, $f_{\epsilon-\delta}^0(r)$, and $g_{\epsilon-\delta}^0(r)$ are (ϵ,δ) independent for $b < r \lesssim \beta_6$, we immediately obtain the conclusion that the K_{ij}^0 $(i,j = o,c)$ are independent of ϵ and δ.

APPENDIX B: CALCULATION OF DISSOCIATION RATE

In this appendix we calculate the dissociation rate of the two-atom bound state and prove Eqs. (60)–(62). In the Schrödinger picture, the Hamiltonian for our problem is given by

$$H = \frac{-\hbar^2\nabla_{\mathbf{R}}^2}{4m} + H_I + H_{\rm rel} + H_{\rm L}, \tag{B1}$$

where $\mathbf{R}$ is the two-atom center-of-mass (c.m.) position. Here H_I describes the one-body internal-state energy and is given by

$$H_I = \sum_{j=1,2}\sum_{l=e,g}\sum_{s=\uparrow,\downarrow} E_{ls}|l\rangle^{(j)}\langle l| \otimes |s\rangle^{(j)}\langle s|, \tag{B2}$$

with E_{ls} $(l = e,g;\ s = \uparrow,\downarrow)$ the one-body energy corresponding to $|l\rangle^{(j)}|s\rangle^{(j)}$, as defined in Sec. III B. In Eq. (B1) $H_{\rm rel}$ and $H_{\rm L}$ are the Hamiltonians for the two-atom relative motion and laser-atom coupling, respectively, and can be expressed as

$$H_{\rm rel} = \frac{-\nabla_{\mathbf{r}}^2}{m} + U(\mathbf{r}), \tag{B3}$$

$$H_{\rm L} = \frac{\hbar\Omega}{2}\sum_{j=1,2} |e\rangle^{(j)}\langle g|e^{i(\mathbf{k}_{\rm L}\cdot\mathbf{r}_j - \omega_{\rm L}t)} + \text{H.c.}, \tag{B4}$$

where $\mathbf{r}$ is the two-atom relative position, $U(\mathbf{r})$ is the total interaction potential defined in Eq. (5), Ω is the Rabi frequency of the clock laser beam, and $\mathbf{k}_{\mathrm{L}}$ and ω_{L} are the wave vector and angular frequency of this laser beam, respectively. In Eq. (B4) $\mathbf{r}_j$ $(j = 1,2)$ is the position of the jth atom and can be expressed as

$$\mathbf{r}_1 = \mathbf{R} + \frac{\mathbf{r}}{2}, \tag{B5}$$

$$\mathbf{r}_2 = \mathbf{R} - \frac{\mathbf{r}}{2}. \tag{B6}$$

As shown in Eq. (58) of Sec. III.B, we assume that at $t = 0$ the two-atom initial wave function is

$$|\Psi(\mathbf{R},\mathbf{r},t=0)\rangle = \frac{1}{(2\pi)^{3/2}} \int d\mathbf{K}\, \phi(\mathbf{K}) e^{i\mathbf{K}\cdot\mathbf{R}} |\phi_b(r)\rangle, \tag{B7}$$

where $|\phi_b(r)\rangle$ is the wave function of the two-atom bound state. We further assume that the laser beam is applied from $t = 0$. Thus, for $t \geqslant 0$ the evolution of the two atoms is governed by the total Hamiltonian H. At time t the two-atom wave function can be denoted by $|\Psi(\mathbf{R},\mathbf{r},t)\rangle$ and the probability of these two atoms being at the bound state $|\phi_b(r)\rangle$ can be expressed as

$$P(t) = \int d\mathbf{R} \left| \int d\mathbf{r} \langle \phi_b(r) | \Psi(\mathbf{R},\mathbf{r},t) \rangle \right|^2. \tag{B8}$$

To calculate $P(t)$ with the Fermi golden rule, we introduce a unitary transformation

$$\mathcal{U} = e^{-i\mathbf{k}_L \cdot \mathbf{R} \Sigma_e}, \tag{B9}$$

where

$$\Sigma_e = |e\rangle^{(1)}\langle e| \otimes |e\rangle^{(2)}\langle e| - |g\rangle^{(1)}\langle g| \otimes |g\rangle^{(2)}\langle g|. \tag{B10}$$

We further define the wave function $|\Phi(\mathbf{R},\mathbf{r},t)\rangle$ as

$$|\Phi(\mathbf{R},\mathbf{r},t)\rangle = \mathcal{U}|\Psi(\mathbf{R},\mathbf{r},t)\rangle, \tag{B11}$$

i.e., $|\Phi(\mathbf{R},\mathbf{r},t)\rangle$ is the two-atom state in the rotated frame induced by $\mathcal{U}$. It is easy to prove that we have

$$|\Phi(\mathbf{R},\mathbf{r},t=0)\rangle = |\Psi(\mathbf{R},\mathbf{r},t=0)\rangle, \tag{B12}$$

$$P(t) = \int d\mathbf{R} \left| \int d\mathbf{r} \langle \phi_b(r) | \Phi(\mathbf{R},\mathbf{r},t) \rangle \right|^2. \tag{B13}$$

Furthermore, we can also prove that $|\Phi(\mathbf{R},\mathbf{r},t)\rangle$ satisfies the Schrödinger equation

$$i\hbar \frac{d}{dt} |\Phi(\mathbf{R},\mathbf{r},t)\rangle = H_{\mathrm{rot}} |\Phi(\mathbf{R},\mathbf{r},t)\rangle, \tag{B14}$$

with H_{rot} the Hamiltonian in the rotated frame, and can be expressed as

$$H_{\mathrm{rot}} = \frac{(-i\hbar\nabla_{\mathbf{R}} + \hbar\mathbf{k}_{\mathrm{L}}\Sigma_e)^2}{4m} + H_I + H_{\mathrm{rel}} + h_{\mathrm{L}}, \tag{B15}$$

with

$$h_{\mathrm{L}} = \frac{\hbar\Omega}{2} e^{-i\omega_{\mathrm{L}}t} (|e\rangle^{(1)}\langle g|e^{i\mathbf{k}_{\mathrm{L}}\cdot\mathbf{r}/2} + |e\rangle^{(2)}\langle g|e^{-i\mathbf{k}_{\mathrm{L}}\cdot\mathbf{r}/2}) + \mathrm{H.c.} \tag{B16}$$

Equation (B15) shows that in the rotated frame the momentum of the c.m. is conserved. Using this fact and Eqs. (B12) and (B7), we can simplify the calculation of the probability $P(t)$ in Eq. (B13) and obtain

$$P(t) = \int d\mathbf{K} |\phi(\mathbf{K})|^2 p(\mathbf{K},t), \tag{B17}$$

where $p(\mathbf{K})$ is given by

$$p(\mathbf{K},t) = \left| \int d\mathbf{r} \langle \phi_{\mathbf{K}}(\mathbf{r},t) | \phi_b(r) \rangle \right|^2. \tag{B18}$$

Here the wave function $|\phi_{\mathbf{K}}(\mathbf{r},t)\rangle$ satisfies the equation

$$i\frac{d}{dt} |\phi_{\mathbf{K}}(\mathbf{r},t)\rangle = h(\mathbf{K}) |\phi_{\mathbf{K}}(\mathbf{r},t)\rangle, \tag{B19}$$

with

$$h(\mathbf{K}) = \frac{-\hbar^2\nabla_{\mathrm{r}}^2}{m} + H_I + U(\mathbf{r}) + \frac{(\hbar\mathbf{K} + \hbar\mathbf{k}_{\mathrm{L}}\Sigma_e)^2}{4m} + h_{\mathrm{L}} \tag{B20}$$

$$\equiv h_0(\mathbf{K}) + h_{\mathrm{L}}, \tag{B21}$$

as well as the initial condition

$$|\phi_{\mathbf{K}}(\mathbf{r},t=0)\rangle = |\phi_b(r)\rangle. \tag{B22}$$

Equations (B18)–(B22) show that to calculate $p(\mathbf{K},t)$ we need to solve a quantum evolution problem governed by the Hamiltonian $h(\mathbf{K})$. This problem is defined in the Hilbert space $\mathcal{H}_r \otimes \mathcal{H}_I$, with $\mathcal{H}_r$ and $\mathcal{H}_I$ the space for the two-atom spatial relative motion and the two-atom internal state, respectively, and the c.m. momentum $\hbar\mathbf{K}$ just behaves as a classical parameter (c-number). In this problem, the term h_{L} induces the transitions from the isolated state $|\phi_b(r)\rangle$, which is a discrete eigenstate of $h_0(\mathbf{K})$, to other continuous eigenstates of $h_0(\mathbf{K})$, i.e., the scattering states of two atoms in either the electronic-orbital state $|e\rangle^{(1)}|e\rangle^{(2)}$ or $|g\rangle^{(1)}|g\rangle^{(2)}$. Thus, we can calculate $p(\mathbf{K},t)$ using Fermi's golden rule and obtain that when the time t is small enough we have [24]

$$p(\mathbf{K},t) = 1 - \gamma(\mathbf{K})t, \tag{B23}$$

where $\gamma(\mathbf{K})$ is given by Eqs. (61) and (62) in Sec. III B. Furthermore, substituting Eq. (B23) into Eq. (B17) and using Eq. (59) in Sec. III B, we can obtain Eq. (60) in Sec. III B.

[1] H. Feshbach, Ann. Phys. (NY) **5**, 357 (1958).

[2] C. Chin, R. Grimm, P. Julienne, and E. Tiesinga, Rev. Mod. Phys. **82**, 1225 (2010).

[3] R. Zhang, Y. Cheng, H. Zhai, and P. Zhang, Phys. Rev. Lett. **115**, 135301 (2015).

[4] G. Pagano, M. Mancini, G. Cappellini, L. Livi, C. Sias, J. Catani, M. Inguscio, and L. Fallani, Phys. Rev. Lett. **115**, 265301 (2015).

[5] M. Höfer, L. Riegger, F. Scazza, C. Hofrichter, D. R. Fernandes, M. M. Parish, J. Levinsen, I. Bloch, and S. Fölling, Phys. Rev. Lett. **115**, 265302 (2015).

[6] R. Zhang, D. Zhang, Y. Cheng, W. Chen, P. Zhang, and H. Zhai, Phys. Rev. A **93**, 043601 (2016).
[7] J. Xu, R. Zhang, Y. Cheng, P. Zhang, R. Qi, and H. Zhai, Phys. Rev. A **94**, 033609 (2016).
[8] L. Isaev, J. Schachenmayer, and A. M. Rey, Phys. Rev. Lett. **117**, 135302 (2016).
[9] S. Capponi, P. Lecheminant, and K. Totsuka, Ann. Phys. (NY) **367**, 50 (2016).
[10] V. Bois, P. Fromholz, and P. Lecheminant, Phys. Rev. B **93**, 134415 (2016).
[11] M. Iskin, Phys. Rev. A **94**, 011604 (2016).
[12] L. He, J. Wang, S.-G. Peng, X.-J. Liu, and H. Hu, Phys. Rev. A **94**, 043624 (2016).
[13] R. Qi, arXiv:1606.03299.
[14] Y.-C. Zhang, S. Ding, and S. Zhang, arXiv:1606.07168.
[15] X. Zhang, M. Bishof, S. L. Bromley, C. V. Kraus, M. S. Safronova, P. Zoller, A. M. Rey, and J. Ye, Science **345**, 1467 (2014).
[16] Y. Cheng, R. Zhang, and P. Zhang, Phys. Rev. A **93**, 042708 (2016).
[17] B. Gao, Phys. Rev. A **58**, 4222 (1998).
[18] B. Gao, E. Tiesinga, C. J. Williams, and P. S. Julienne, Phys. Rev. A **72**, 042719 (2005).
[19] B. Gao, Phys. Rev. A **80**, 012702 (2009).
[20] B. Gao, Phys. Rev. A **84**, 022706 (2011).
[21] B. Gao, Phys. Rev. A **58**, 1728 (1998). The functions $f^0_{\epsilon,l=0}(r)$ and $g^0_{\epsilon,l=0}(r)$ in this reference are denoted, respectively, by $f^0_\epsilon(r)$ and $g^0_\epsilon(r)$ in this paper.
[22] B. Gao, Phys. Rev. A **62**, 050702(R) (2000).
[23] B. Gao, Phys. Rev. A **64**, 010701(R) (2001).
[24] Precisely speaking, Fermi's golden rule is applicable when both of the following two conditions are satisfied: (a) t is short enough so that the atom-laser coupling can be considered as a lowest-order perturbation and (b) t is much longer than the correlation time of the laser-induced coupling between the bound state and the scattering states.
[25] G. Cappellini, M. Mancini, G. Pagano, P. Lombardi, L. Livi, M. Siciliani de Cumis, P. Cancio, M. Pizzocaro, D. Calonico, F. Levi, C. Sias, J. Catani, M. Inguscio, and L. Fallani, Phys. Rev. Lett. **113**, 120402 (2014).
[26] F. Scazza, C. Hofrichter, M. Höfer, P. C. De Groot, I. Bloch, and S. Fölling, Nat. Phys. **10**, 779 (2014).
[27] L. Jiang, H. Pu, W. Zhang, and H. Y. Ling, Phys. Rev. A **80**, 033606 (2009).
[28] Z. Fu, P. Wang, L. Huang, Z. Meng, and J. Zhang, Phys. Rev. A **86**, 033607 (2012).
[29] L. Huang, P. Wang, P. Peng, Z. Meng, L. Chen, P. Zhang, and J. Zhang, Phys. Rev. A **91**, 041604(R) (2015).